# Assessing local and long-range structural disorder in aggregate-free lime binders

Ben Xu,[†,§] Michael B. Toffolo,[‡,‖] Elisabetta Boaretto,[‡] and Kristin M. Poduska[*,¶]

[†]*Department of Physics and Physical Oceanography, Memorial University of Newfoundland, St. John's, NL, Canada,* [‡]*Max Planck Weizmann Center for Integrative Archaeology and Anthropology, Weizmann Institute of Science, Rehovot, Israel, and* [†]*Department of Physics and Physical Oceanography, Memorial University of Newfoundland, NL, Canada*

E-mail: kris@mun.ca

[*]To whom correspondence should be addressed

[††]Department of Physics and Physical Oceanography, Memorial University of Newfoundland, St. John's, NL, Canada

[‡‡]Max Planck Weizmann Center for Integrative Archaeology and Anthropology, Weizmann Institute of Science, Rehovot, Israel

[¶†]Department of Physics and Physical Oceanography, Memorial University of Newfoundland, NL, Canada

[§]Current address: Department of Science, China University of Petroleum (East China)

[‖]Current address: Institut für Naturwissenschafliche Archäologie, Eberhard Karls Universit ät Tübingen, Tübingen 72070, Germany

**Abstract**

For aggregate-free, calcite-containing lime binders, we correlate long-range crystallinity parameters from X-ray diffraction measurements (lattice constants, crystalline domain sizes, and microstrain fluctuation values) with short-range structural parameters from extended X-ray absorption fine structure data (coordination environments, attenuation factors, and fit stabilities). In doing so, we reveal a correlation between unit cell contraction and a more ideal local calcite structure. Using Fourier transform infrared spectroscopy and X-ray absorption near edge spectroscopy, we rule out the possibility of contributions from amorphous calcium carbonate, and show that the structural disorder is likely related to localized regions of incomplete carbonation. Thus, by using data from this judicious combination of structural characterization tools, we demonstrate that short-range structural distortions occur in calcitic lime binders, and that these distortions can be detected even in multi-phase mixtures.

# Introduction

The carbonation process of calcium-containing minerals holds considerable scientific and industrial interest because the interconversion among different solid phases controls the physical and chemical properties of the end product. For common construction materials such as concrete, mortar, cement, or lime binders, their physical and chemical properties are strongly dependent on the way that CaO ("quicklime" or "free lime") and $Ca(OH)_2$ (portlandite) are converted to $CaCO_3$.[1–6] Previous reports demonstrate that the carbonation rate is strongly influenced by factors such as $CO_2$ concentration, temperature, and relative humidity.[7–11] Furthermore, once the carbonation process begins on the outer surface of a CaO grain, the rate and efficiency of subsequent carbonation are affected by how easily $Ca^{2+}$ and $OH^-$ can permeate the newly-formed $CaCO_3$ coating.[12] The carbonation process is even more complicated when CaO is mixed with silicate hydrates, as is the case while fresh concrete is curing.[13]

Even in the relatively simple case of aggregate-free lime binders, mixtures of phases and polymorphs are commonplace. This is not surprising once one considers the overall reaction progression that produces a lime binder (Equations 1-4).

$$CaCO_3 \xrightarrow{750\ ^\circ C} CaO\ \text{(quicklime)} + CO_2 \quad \text{(Eq. 1)}$$

$$2\ CaO + H_2O \longrightarrow Ca(OH)_2\ \text{(portlandite)} \quad \text{(Eq. 2)}$$

$$Ca(OH)_2 + H_2O \longrightarrow Ca^{2+}_{(aq)} + OH^-_{(aq)} \quad \text{(Eq. 3)}$$

$$Ca^{2+}_{(aq)} + CO^{2-}_{3\ (aq)} \longrightarrow CaCO_3\ \text{(lime binder)} \quad \text{(Eq. 4)}$$

CaO can be produced from any polymorph of calcium carbonate by heating above 750 °C.[14] Upon exposure to water (slaking), quicklime hydrates to portlandite ($Ca(OH)_2$). In the last stage, portlandite carbonates to form $CaCO_3$ through a dissolution and reprecipitation process.[3,8,12] Recent studies found that four different $CaCO_3$ polymorphs (calcite, aragonite, vaterite, and amorphous calcium carbonate) can form from quicklime that is exposed to different relative humidities while at 80°C, without slaking.[7] Even with slaking, calcite-aragonite mixtures can form over a wide variety of ambient humidity and $CO_2$ levels.[15] In this work, we adopt standard plaster process terminology by referring to this kind of multi-phase, unslaked heated product as "lime", while the slaked product we call "lime binder".[14]

Since lime binders are expected to be multi-phase materials, X-ray diffraction (XRD) is a widely used characterization technique. It has great value for sample assessments because the differences in peak positions and widths can be quantified to provide a variety of structural information. For example, growth rates of calcite particles contained in lime binders, obtained from analyses of XRD peak widths, have shown that grains reach a limiting size within a span of hours.[16] A more recent study used *in situ* XRD to identify a two-stage carbonation process that is affected by reaction temperatures.[17] Other XRD studies have focused on lattice expansion differences in lime binder as a function of time and relative humidity.[18] It is much less common to use XRD to assess several different types of structural disorder at the same time. A recent study showed that lattice strain, microstrain fluctuations, and small crystalline domain sizes need to be considered all together, since these

different origins for structural disorder do not influence XRD data in independent ways.[19] The same XRD analysis method has been used to track changes in calcite crystal growth when there are polymeric inclusions.[20]

Despite the advantages of XRD for structural characterization, there is some information that it cannot provide. For example, poorly crystalline and amorphous components cannot be quantified with XRD. However, they can be detected easily with Fourier transform infrared (FTIR) spectroscopy or with Raman spectroscopy.[21] Nevertheless, these vibrational spectroscopy techniques are not applied routinely to lime binders.[7,22] In the case of extremely disordered or amorphous materials, synchrotron-based X-ray absorption fine structure (XAFS) measurements are the benchmark for assessing local atomic coordination environments.[23] XAFS is a comprehensive term that includes both data in the immediate vicinity of the absorption edge (X-ray absorption near edge, XANES), as well as information at energies high above the absorption edge (extended X-ray absorption fine structure, EXAFS). Although XAFS has been widely applied to biogenic carbonates,[23–26] there is a distinct lack of data about the local chemical environment of lime binders.

In this work, we demonstrate the advantages of using a combination of bulk (XRD and FTIR) and local (XAFS) structural characterization tools for lime binders, by showing that the crystalline calcite portion of lime binder exhibits multiple types of structural disorder. Furthermore, the lattice strains and microstrain fluctations that we detect in calcite coincide with the presence of $Ca(OH)_2$. These results are important because they suggest that incomplete carbonation causes distinctive structural disorder characteristics in lime binders.

# Experimental details

Our goal was to demonstrate that we can detect structural disorder signatures in aggregate-free, calcite-containing lime binders that contain a complex mixture of phases and polymorphs. To do this, we needed to prepare the quicklime starting material, and then to

coordinate the timing for each of the characterization measurements to ensure that we captured structural information for multi-phase binders.

## Sample preparation

We prepared lime binders using the steps outlined in Equations 1-4. Details for all samples are listed in Table 1. Four different sources of raw calcium carbonate served as starting materials: analytical grade calcite powder from Merck (sample label CP), geogenic calcite spar from Chihuahua, Mexico (CC), geogenic aragonite spar from Minglanilla, Spain (CA), and bivalve shells *Glycymeris insubrica* from Ashkelon, Israel (GA). Different quicklime samples were produced by heating 5 g of starting material for 12 hours at 900 °C in an electric muffle oven with an ambient air atmosphere. This duration was sufficient to ensure complete conversion of the starting material to CaO; representative FTIR data for quicklime are included in Supporting Information Figure S1. After heating, the samples were quenched to room temperature in ambient air. The resulting powders were then slaked by mixing with excess deionized water (about 10 times by volume) in glass beakers. The resulting lime binder samples (BP900, BC900, BA900, BG900) were each ∼5 $cm^2$ and ∼3 mm thick. All samples were stored unsealed under ambient conditions that were not monitored. Additional samples (BP800, BC800, BA800, BG800) were prepared using quicklime that was produced by heating calcium carbonate at a lower calcination temperature (800 °C). A 12 hour heating duration was still sufficient to ensure complete conversion of the starting material to CaO (see Supporting Information Figure S1). Spar calcite (CC) and aragonite (CA) served as standards, along with a fully carbonated, well-crystallized ancient binder from Yiftahel, Israel (BY).[27,28]

## Structural characterization

FTIR data were our primary method for assessing when the lime binders had a sufficient amount of calcite to proceed with other characterization methods. Transmission FTIR spec-

Table 1: Sample details, including raw starting materials and calcination temperatures. All lime binders were calcined for 12 hours.

| **Sample name** | **Raw source material** | **Calcining T (°C)** |
|---|---|---|
| **standards** | | |
| CP | purchased calcite | — |
| CC | spar calcite | — |
| BY | ancient lime binder (Yiftahel) | — |
| CA | spar aragonite | — |
| **lime binders** | | |
| BP800 | purchased calcite | 800 |
| BC800 | spar calcite | 800 |
| BA800 | spar aragonite | 800 |
| BG800 | glycymeris | 800 |
| BP900 | purchased calcite | 900 |
| BC900 | spar calcite | 900 |
| BA900 | spar aragonite | 900 |
| BG900 | glycymeris | 900 |

tra came from samples that were ground together with spectrophotometric grade KBr (1:50 ratio), and then pressed into 3 mm diameter pellets using 2 tons of pressure from a torque wrench. Our spectra were acquired using a Bruker Vertex 70v/S vacuum spectrometer with a globar IR source (4000-500 $cm^{-1}$ collection range at 1 $cm^{-1}$ resolution).

Approximately 1 week prior to XAFS measurements, we collected XRD data on hand-powdered samples using a Rigaku Ultima IV diffractometer (Cu K$\alpha$, 20-70° $2\theta$ range, 0.02° step size, 1 s dwell time). Using the JADE 7.0 software to fit peak widths and positions, we calculated lattice constants, crystalline domain sizes, and microstrain fluctuation values using a procedure described in more detail elsewhere.[19]

Finally, XAFS measurements were conducted on the Soft X-ray Micro-characterization Beamline 06B1-1 at the Canadian Light Source in Saskatoon, SK, Canada. In our XAFS experiments, Ca $K$-shell electrons absorb X-ray photons, leaving core holes when they are ejected. The higher-energy electrons that fill the holes will emit photons. Both the ejected electrons and emitted photons were detected in our experiments; the XAFS spectra we show here are based on total electron yield.

XAFS data were measured 8 months after the lime binders were slaked, which was enough

time for sufficient calcite to form, but while there was still some $Ca(OH)_2$ present. A small quantity of powdered lime binder was mounted on carbon tape attached to a copper plate. Samples were then exposed to synchrotron X-rays with a range of energies below and above the Ca K-edge (4038 eV) to measure differences in the ejected electron and photon fluxes as a function of incident X-ray energy. The resulting XAFS data were processed and analyzed using the IFEFFIT software package.[29]

In the near-edge (XANES) region (4030–4043 eV), data were compared directly. In the extended (EXAFS) region (4043–4188 eV), the subsequent data analyses were very extensive. Fourier transforms of EXAFS spectra in $k$ space were based on data for 2-9 $Å^{-1}$. The Artemis software (FEFF8)[29] allowed us to develop a model of ideal calcite that we could compare with our data, including coordination number, neighbor distances ($r$), and deviations in distance due to structural disorder ($\sigma^2$). Our fitting ranges for real-space transformations is 1-4 Å, which includes the first four coordination shells.

# Results

## Phase compositions from bulk analyses

Since poorly crystalline phases do not produce definitive diffraction peaks, we used vibrational spectroscopy as our initial structural characterization tool. Figure 1 shows representative FTIR spectra in the mid-IR range for standards, as well as lime binder. The three characteristic peaks of calcite ($\nu_2$, $\nu_3$, and $\nu_4$) are present in all samples.[21] Lime binder shows a strong peak near 3643 $cm^{-1}$ that is due to $OH^-$ stretching in $Ca(OH)_2$. A weak peak at 855 $cm^{-1}$ in some lime binder spectra is due to aragonite. No signs of other phases, such as amorphous calcium carbonate, were visible. We note that our FTIR spectra cannot show evidence of CaO because the vibrational modes of this material lie at lower wavenumbers (less than 500 $cm^{-1}$).

To assess the crystalline content of our samples, we compared powder XRD data with

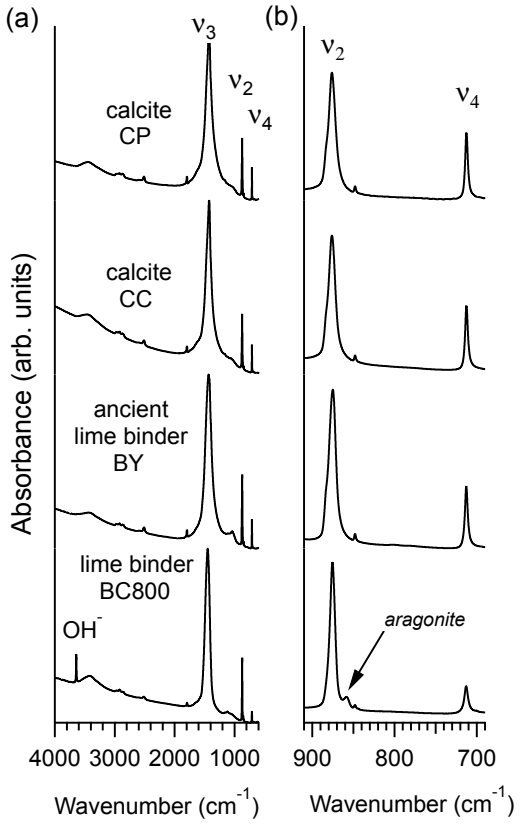


Figure 1: Representative FTIR spectra (a) in the full mid-IR range (4000 $\mathrm{cm}^{-1}$ to 500 $\mathrm{cm}^{-1}$), and (b) a zoom in the calcite fingerprint region (900 $\mathrm{cm}^{-1}$ to 700 $\mathrm{cm}^{-1}$). Spectra are offset along the vertical axis for clarity. For all samples, the $\nu_3$, $\nu_2$, and $\nu_4$ peaks for calcite are dominant. The $\mathrm{OH}^-$ stretching mode in spectra for BC800 indicates $\mathrm{Ca(OH)_2}$. Small amounts of aragonite are detectable in most of our lime binders.

JCPDS standards[30] for calcite (86-2334), aragonite (76-0606), $Ca(OH)_2$ (87-0673), and CaO (82-1691). All eight lime binders contain calcite and $Ca(OH)_2$, plus weak peaks that are related to aragonite, consistent with our FTIR data (Figure 1) and as noted in earlier reports.[15] The ancient lime binder (BY) is composed of well-crystallized calcite. A minor peak near 27° ($2\theta$) suggests that sample BY contains a small amount of a second crystalline phase, but this single peak was not sufficient for identification. None of the lime binders showed evidence of CaO. For completeness, we also analyzed pure aragonite (CA), two different pure calcites (CP, CC), and several unslaked limes. Representative XRD data for all samples are included in Supporting Information Figure S2.

Using these XRD data, we focused on the calcite portion of the samples. Least-squares fits of the XRD peak positions gave us calcite lattice constants ($a$ and $c$, in space group $R\bar{3}c$). Crystalline domain sizes and microstrain fluctuation values were calculated in a correlated way (using Williamson-Hall analyses), since XRD peak widths are affected by both of these factors.[19,20] Comparisons of all XRD-derived calcite crystallinity parameters are summarized in Table 2.

Table 2: Calcite lattice constants ($a$ and $c$), crystalline domain sizes, and microstrain fluctuation values for lime binders and control samples, determined from XRD data.

| sample | $a$ (Å) | $c$ (Å) | size (Å) | microstrain (%) |
|---|---|---|---|---|
| CP | 4.9938 ± 0.0006 | 17.076 ± 0.002 | 900 ± 100 | -0.02 ± 0.02 |
| CC | 4.9851 ± 0.0001 | 17.050 ± 0.003 | >2000 | 0.08 ± 0.07 |
| BY | 4.99 ± 0.02 | 17.0566 ± 0.0004 | 1700 ± 400 | 0.03 ± 0.01 |
| BP800 | 5.002 ± 0.003 | 17.055 ± 0.004 | 330 ± 50 | -0.07 ± 0.04 |
| BC800 | 4.998 ± 0.001 | 17.065 ± 0.001 | 380 ± 60 | 0.03 ± 0.04 |
| BA800 | 4.992 ± 0.002 | 17.061 ± 0.006 | 400 ± 90 | 0.07 ± 0.05 |
| BG800 | 5.002 ± 0.001 | 17.081 ± 0.006 | 400 ± 100 | -0.06 ± 0.07 |
| BP900 | 4.992 ± 0.002 | 17.020 ± 0.008 | 400 ± 100 | 0.03 ± 0.06 |
| BC900 | 4.981 ± 0.009 | 16.99 ± 0.02 | 1100 ± 800 | 0.29 ± 0.07 |
| BA900 | 4.993 ± 0.002 | 17.023 ± 0.008 | 600 ± 100 | 0.14 ± 0.03 |
| BG900 | 4.992 ± 0.002 | 17.01 ± 0.01 | 400 ± 200 | 0.0 ± 0.1 |

## Local chemical structure from XAFS analyses

The pre-edge and XANES region of XAFS spectra are affected by the local chemical environment around all Ca atoms in a specimen. Therefore we compared spectral differences near the Ca $K$-edge (4038 eV) to confirm the content of the mixtures identified from the XRD and FTIR analyses. This consistency check is an important prerequisite before attempting to interpret the extended range (EXAFS) data.

### Pre-edge and near-edge data

Figure 2 compares representative lime binder (BC800), ancient binder (BY), calcite (CC), and aragonite (CA) spectra near the Ca $K$-edge. The small pre-edge peak (a) at 4040 eV and the shoulder (b) at 4045 eV are attributed to the *1s-3d* and $1s$-$4s$ transitions in Ca,[24,25] and these appear in all of our samples. The two main peaks at 4048 eV (c) and 4061 eV (d), are characteristic of calcite. A sharp peak at 4051 eV (e) is due to $Ca(OH)_2$.[31] Aragonite has a large peak that overlaps with calcite's main peak, but it has a unique shoulder (f) that appears in many of our binder spectra, consistent with FTIR data. Thus, lime binder spectra show mixed features of calcite, aragonite, $Ca(OH)_2$, which is consistent with XRD and FTIR data.

### Fine-structure (EXAFS) data

During XAFS measurements, ejected electrons scatter from nearby atoms. Thus, with appropriate background removal, we extracted the spectral oscillations that appear at energies far above the absorption edge, which contain valuable information about the local Ca bonding environment.

By taking Fourier transforms of data at energies higher than the Ca K-edge, we compared scattering intensities that are directly related to the real-space distances of the Ca nearest neighbours (coordination shells). It is important to note that the positions of these EXAFS peaks do not represent the true bond distances because there are phase corrections inherent to

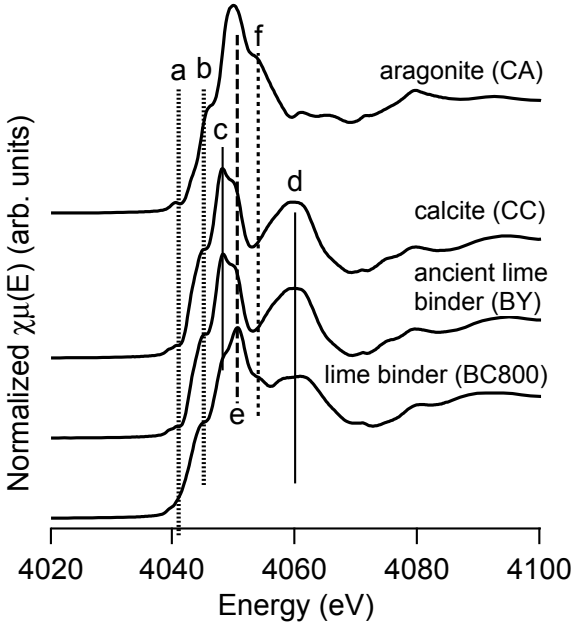


Figure 2: Representative XAFS data near the Ca $K$-edge for aragonite (CA), calcite (CC), ancient binder (BY), modern lime binder (BC800), and unslaked lime. Spectra are offset along the vertical axis for clarity. The pre-edge absorption peak (a) and shoulder (b) are due to atomic transitions in Ca, so they appear in all of our spectra. Two XANES peaks (c and d) are characteristic of calcite. Peaks indicative of $Ca(OH)_2$ (e) and aragonite (f) are present in modern lime binders.

the Fourier transformations.[32] For this reason, we follow the standard practice of comparing the relative positions of EXAFS peaks, using identical ranges, transformation parameters, and phase corrections for each spectrum. In all EXAFS plots, the Ca-Ca peak for calcite occurs near 3.5 Å, and this peak is largest in our calcite standards (CP, CC, and BA). On the other hand, Ca-Ca neighbours in $Ca(OH)_2$ produce a strong peak at 2.9 Å that appears in all lime binders. This portlandite-related peak is much weaker in the 900 °C lime binders.

Our data (such as the representative spectra shown in Figure 3) compare well with EXAFS data simulated for ideal calcite, which we generated using the Artemis analysis package[29] with established crystallographic parameters for calcite.[33] Our analyses included the first four coordination shells (Ca-$O_1$, Ca-C, Ca-$O_2$, and Ca-Ca), and we used fixed coordination numbers. The variable parameters during fitting were bond distance ($r$), the variance in the half scattering path length ($\sigma^2$), and the amplitude. Figure S3 and Table S1 in the Supporting Information summarize the EXAFS results.

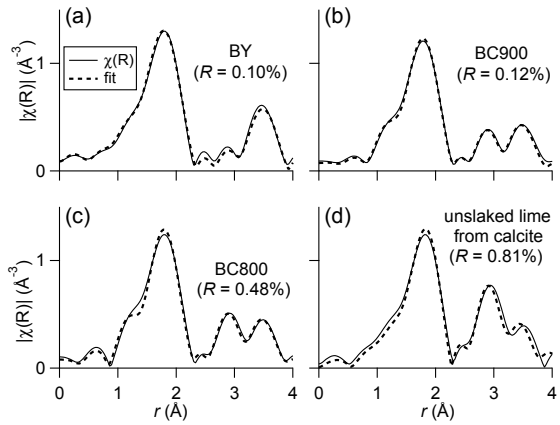


Figure 3: Representative Fourier-transformed EXAFS spectra for (a) ancient lime binder, (b) 900 °C lime binder, (c) 800 °C lime binder. For comparison, an unslaked lime is shown in (d). Dashed lines indicate fitted results based on ideal calcite using four coordination shells, and $R$-factors (%) are included in parentheses.

Bonding distances for all samples are consistent with those from standard crystallographic data for calcite.[33] However, the $R$-factors, which are related to the stability of the EXAFS fit, show systematic variations (all data are included in Supporting Information Table S1). Lime binder samples calcined at lower temperatures (800 °C) have consistently larger $R$-factors,

indicating a poorer match with pure calcite.

# Discussion

It is well known that lime binders can include several different phases (aragonite, calcite, CaO, $Ca(OH)_2$, and amorphous calcium carbonate), and that the composition can change during the curing process. In this study, our lime binders were not fully cured, and they contained three of these phases: calcite, aragonite, and $Ca(OH_2)$. When assessing the EXAFS spectra, some lime binders were comparable to our calcite standards, while others exhibited a much poorer match to pure calcite. It is tempting to assume that the higher $R$-factors (poorer fits) for some lime binder spectra is a simple consequence of their multi-phase compositions. However, by comparing EXAFS $R$-factors with data from the XRD analyses, we find that the situation is much more interesting.

We compared the microstrain fluctuation value, crystalline domain size, and $c$-lattice constant against $R$-factors for all lime binder samples (Figure 4). Most notably, we find that not all crystallinity parameters are correlated with changes in $R$-factor. Consistent with earlier reports, we find that the calcination temperature is important.[7,14,15] Lime binders calcined at higher temperatures (900 °C) have larger crystalline domain sizes and also larger microstrain fluctuation values. However, the higher calcination temperatures also correlate with a contraction of the calcite lattice, especially along the $c$ direction. In fact, the $c$-lattice constant values show the clearest direct correlation with the $R$-factor values. In other words, a more contracted $c$-lattice, even when considerably smaller than the calcite standard, coincides with the best *local* calcite coordination environment.

To explain these trends, we put our work in the context of literature that has examined the progression of phase conversions during the lime binder carbonation process. Our results are consistent with other reports that show, at the beginning of this carbonation process, that the small calcite crystals have lattice constants that are close to those for ideal calcite

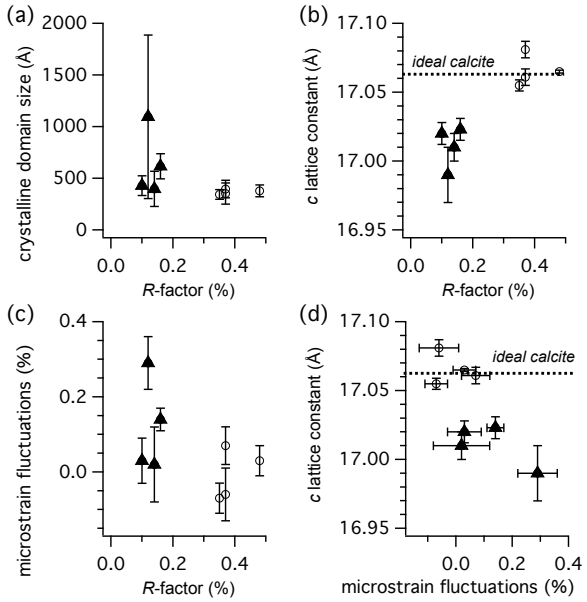


Figure 4: *R*-factors from EXAFS fits for lime binder samples correlated with different crystallinity parameters from XRD data: (a) for crystalline domain size, (b) for *c*-lattice constant, and (c) for microstrain fluctuations. The correlation between *c*-lattice constant and microstrain fluctuations is shown in (d). In all plots, the solid triangles denote calcination 900°C, and the hollow circles signify 800°C calcination. In (b) and (d), the ideal *c*-lattice parameter is based on JCPDS standard pattern 86-2334.[30]

(JCPDS 86-2334).[17,20] However, our results suggest that subsequent stages of crystallite growth tend to occur in a more imperfect way, since microstrain fluctuations values grow and the *c*-lattice constants shrink. This is consistent with recent reports that larger calcite crystallites, similar in size to ours (near 500 nm) but grown with polymeric inclusions, also show larger microstrain fluctuations.[20] We propose that $Ca(OH)_2$ inclusions, related to non-uniform carbonation, could serve a similar role as the polymeric inclusions, decreasing the *c*-lattice constants and contributing to larger microstrain fluctuation values.

Earlier reports[20] do not speculate why crystallite size and lattice strain are correlated in calcite, and it is not addressed directly in the existing literature. In other subdisciplines, XAFS has provided critical insights on the crystallization processes of calcite from biogenic and lab-produced amorphous calcium carbonate (ACC).[23–25,34] Unstable EXAFS fits in ACC (resulting in large reduced $\chi^2$ values, which are a measure of goodness of fit that are similar to our *R*-factors) have been attributed to heterogeneities in the Ca coordination shells.[23] A recent report has also shown evidence of ACC in lime binders.[7] However, the lime binders in our study are considerably different from ACC. Most notably, they show prominent XRD peaks that indicate crystalline calcite, and there is no evidence of ACC in our lime binder FTIR spectra. Thus, higher *R*-factors in our calcitic lime binders are not linked with the presence of amorphous calcium carbonate.

# Conclusions

Calcite-containing lime binders are complex, mixed-phase materials. Nevertheless, our work demonstrates that distinctive types of structural disorder within the calcite can be identified and quantified. By combining XRD and XAFS data, we show that short-range structural distortions occur in calcitic lime binders, and that the lattice strains and microstrain fluctations that we detect in calcite coincide with the presence of $Ca(OH)_2$.

Although it is not necessarily surprising that $Ca(OH)_2$ inclusions can contribute to dis-

tortions in calcite-containing lime binders, it is interesting that the overall mix of disorder (lattice expansions, microstrain fluctuations, and crystalline domain sizes) can be different from what has been reported in calcite produced by other methods. For example, large-grained calcitic flowstones from cave environments have shown contracted lattices and a varied range of microstrain fluctuation values.[19] On the other hand, recent laboratory-produced calcite with polymeric inclusions have shown qualitatively similar microstrain fluctuation and crystalline domain size correlations, though with generally smaller microstrain fluctuation values.[20] Furthermore, these two studies,[19,20] along with the present work, are among the few to emphasize that there are several possible origins for line broadening in calcite XRD spectra. This is especially important for studies of lime binder if one wants to follow the growth and evolution of grains within a specimen under different curing conditions.

Our study reveals useful information about lime binders that should stimulate future investigations as well. For example, we suspect that changes in lattice constants and microstrain fluctuation values could help track changes in the mechanical strength of pure lime binders (as well as aggregate-containing variants such as cements, concretes, plasters, and mortars) during the curing process. This could be especially important for repairs to historic structures, since a plaster binder that is either to strong or too weak will create new problems rather than solving existing ones.[2,3] Strength and fracture properties of lime-based materials are known to be influenced by porosity, and this can be affected by factors such as aggregate concentration, polymeric inclusions, and rheological properties of the lime putty before it hardens.[1,2,5,6] Nevertheless, it remains to be investigated whether there is a link between porosity and crystal structure disorder in lime binders.[1] There are good reasons to explore this possibility, since porosity and micro-cracks have been shown to affect microstrain fluctuation values in biogenic calcium carbonate.[35,36] Thus, the tools and analysis strategy we present here offer possibilities for better understanding of calcium carbonate polymorphs and related phases in lime binders.

## Acknowledgement

A portion of the research described in this paper was performed at the Canadian Light Source (CLS), which is supported by the Canada Foundation for Innovation, Natural Sciences and Engineering Research Council of Canada, the University of Saskatchewan, the Government of Saskatchewan, Western Economic Diversification Canada, the National Research Council Canada, and the Canadian Institutes of Health Research. We thank Dr. Y. Hu, Dr. L. Maclean, and A. Maclennan at the SXRM beamline at CLS, and BX acknowledges CLS for student travel funds. XRD measurements were completed with the help of Dr. W. Aylward (CREAIT facilities, Memorial University). This work was funded through an NSERC (Canada) Discovery Grant (KMP).

## Supporting Information Available

FTIR data for quicklime, powder X-ray diffraction data, EXAFS spectra, EXAFS fitting results.

This material is available free of charge via the Internet at `http://pubs.acs.org/`.

## References


(1) Rieger, J.; Kellermeier, M.; Nicoleau, L. Formation of nanoparticles and nanostructures. *Angew. Chem. Int. Ed.* **2014**, *53*, 12380.

(2) Válek, J., Hughes, J. J., Groot, C. J. W. P., Eds. *Historic mortars*; Springer, 2012.

(3) Elert, K.; Rodriguez-Navarro, C.; Pardo, E. S.; Hansen, E.; Cazalla, O. Lime Mortars for the Conservation of Historic Buildings. *Studies in Conservation* **2002**, *47*, 62.

(4) Stefanidou, M.; Papayianni, I. The role of aggregates on the structure and properties of lime mortars. *Cement Concrete Comp.* **2005**, *27*, 914.

(5) Ruiz-Agudo, E.; Rodriguez-Navarro, C. Microstructure and Rheology of Lime Putty. *Langmuir* **2009**, *26*, 3868.

(6) Aradigoyen, M.; Alvarez, J. I. Pore structure and mechanical properties of cement-lime mortars. *Cement Concrete Res.* **2007**, *37*, 767.

(7) Dubina, E.; Korat, L.; Black, L.; Strupi-Šuput, J.; Plank, J. Influence of water vapour and carbon dioxide on free lime during storage at $80°C$, studied by Raman spectroscopy. *Spectrochim. Acta Part A* **2013**, *111*, 299.

(8) Huntzinger, D. N.; Gierke, J. S.; Kawatra, S. K.; Eisele, T. C.; Sutter, L. L. Carbon Dioxide Sequestration in Cement Kiln Dust through Mineral Carbonation. *Environ. Sci. Technol.* **2009**, *43*, 1986.

(9) Dheilly, R. M.; Tudo, J.; Sebaíbi, Y.; Quéneudec, M. Influence of storage conditions on the carbonation of powdered $Ca(OH)_2$. *Construct. Build. Mater* **2002**, *16*, 155.

(10) García-Labiano, F.; Abad, A.; de Diego, L.; Gayán, P.; Adánez, J. Calcination of calcium-based sorbents at pressure in a broad range of $CO_2$ concentrations. *Chem. Eng. Sci.* **2002**, *57*, 2381.

(11) Abanades, J. C. The maximum capture efficiency of $CO_2$ using a carbonation/calcination cycle of $CaO/CaCO_3$. *Chem. Eng. J.* **2002**, *90*, 303.

(12) Galan, I.; Glasser, F.; Baza, D.; Andrade, C. Assessment of the protective effect of carbonation on portlandite crystals. *Cement Concrete Res.* **2015**, *74*, 68.

(13) Kashef-Haghighi, S.; Ghoshal, S. Physical-chemical Processes Limiting $CO_2$ Uptake in Concrete during Accelerated Carbonation Curing. *Ind. Eng. Chem. Res.* **2013**, *52*, 5529.

(14) Boynton, R. S. *Chemistry and technology of lime and limestone*; John Wiley & Son, Inc., New York, 1980.

(15) Toffolo, M. B.; Boaretto, E. Nucleation of aragonite upon carbonation of calcium oxide and calcium hydroxide at ambient temperatures and pressures: a new indicator of fire-related human activities. *J. Archaeolog. Sci.* **2014**, *49*, 237.

(16) Montes-Hernandez, G.; Fernández-Martínez, A.; Renard, F. Novel Method to Estimate the Linear Growth Rate of Submicrometric Calcite Produced in a Triphasic Gas-Liquid-Solid System. *Cryst. Growth Des.* **2009**, *9*, 4567.

(17) Biasin, A.; Segre, C. U.; Strumendo, M. $CaCO_3$ Crystallite Evolution during CaO Carbonation: Critical Crystallite Size and Rate Constant Measurement by In-Situ Synchrotron Radiation Xray Powder Diffraction. *Cryst. Growth Des.* **2015**, *15*, 5188.

(18) Gomez-Villalba, L.; López-Arce, P.; Alvarez de Buergo, M.; Fort, R. Structural stability of a colloidal solution of $Ca(OH)_2$ nanocrystals exposed to high relative humidity conditions. *Appl. Phys. A* **2011**, *104*, 1249.

(19) Xu, B.; Toffolo, M. B.; Regev, L.; Boaretto, E.; Poduska, K. M. Structural differences in archaeologically relevant calcite. *Anal. Methods* **2015**, *7*, 9304.

(20) Kim, Y.-Y.; Schenk, A. S.; Ihli, J.; Kulak, A. N.; Hetherington, N. B. J.; Tang, C. C.; Schmahl, W. W.; Griesshaber, E.; Hyett, G.; Meldrum, F. C. A critical analysis of calcium carbonate mesocrystals. *Nature Comm.* **2014**, *5*, 4341..

(21) Weiner, S. *Microarchaeology: Beyond the visible archaeological record*; Cambridge University Press, 2010.

(22) Boaretto, E.; Poduska, K. M. Materials Science Challenges in Radiocarbon Dating: The Case of Archaeological Plasters. *J. Mater.* **2013**, *65*, 481.

(23) Levi-Kalisman, Y.; Raz, S.; Weiner, S.; Addadi, L.; Sagi, I. Structural Differences Between Biogenic Amorphous Calcium Carbonate Phases Using X-ray Absorption Spectroscopy. *Adv. Funct. Mater.* **2002**, *12*, 43.

(24) Politi, Y.; Levi-Kalisman, Y.; Raz, S.; Wilt, F.; Addadi, L.; Weiner, S.; Sagi, I. Structural characterization of the transient amorphous calcium carbonate precursor phase in sea urchin embryos. *Adv. Funct. Mater.* **2006**, *16*, 1289.

(25) Lam, R. S. K.; Charnock, J. M.; Lennie, A.; Meldrum, F. C. Synthesis-dependant structural variations in amorphous calcium carbonate. *Cryst. Eng.* **2007**, *9*, 1226.

(26) Gebauer, D.; Gunawidjaja, P. N.; Ko, J. Y. P.; Bacsik, Z.; Aziz, B.; Liu, L.; Hu, Y.; Bergstrom, L.; Tai, C.-W.; Sham, T.-K.; Eden, M.; Hedin, N. Proto-Calcite and Proto-Vaterite in Amorphous Calcium Carbonates. *Angew. Chem. Int. Ed.* **2010**, *49*, 8889.

(27) Regev, L.; Poduska, K. M.; Addadi, L.; Weiner, S.; Boaretto, E. Distinguishing between calcites formed by different mechanisms using infrared spectrometry: archaeological applications. *J. Archaeolog. Sci.* **2010**, *37*, 3022.

(28) Poduska, K. M.; Regev, L.; Boaretto, E.; Addadi, L.; Weiner, S.; Kronik, L.; Curtarolo, S. Decoupling Local Disorder and Optical Effects in Infrared Spectra: Differentiating Between Calcites with Different Origins. *Adv. Mater.* **2011**, *23*, 550.

(29) Ravel, B.; Newville, M. ATHENA, ARTEMIS, HEPHAESTUS: data analysis for X-ray absorption spectroscopy using IFEFFIT. *J. Synchrotron Radiat.* **2005**, *12*, 537.

(30) *Joint Commission on Powder Diffraction Standards, International Centre for Diffraction Data, http://www.icdd.com* **2003**.

(31) Sowrey, F. E.; Skipper, L. J.; Pickup, D. M.; Drake, K. O.; Lin, Z.; Smith, M. E.; Newport, R. J. Systematic empirical analysis of calcium-oxygen coordination environment by calcium K-edge XANES. *Phys. Chem. Chem. Phys.* **2004**, *6*, 188.

(32) Newville, M. Fundamentals of X-ray absorption fine structure. *Consortium for Advanced Radiation Sources, University of Chicago (USA), http://xafs.org* **2004**.

(33) Markgraf, S. A.; Reeder, R. J. High-temperature structure refinements of calcite and magnesite. *Am. Mineral.* **1985**, *70*, 590.

(34) Loste, E.; Wilson, R. M.; Seshadri, R.; Meldrum, F. C. The role of magnesium in stabilising amorphous calcium carbonate and controlling calcite morphologies. *J. Cryst. Growth* **2003**, *254*, 206.

(35) Yan, X.-H.; Wang, S.-N.; Zhang, X.-J.; Wang, X.-X.; Wang, R. Arrangement of intracrystalline organic matrix in nacre from red abalone: A view by high-resolution synchrotron powder diffraction combined with SEM observation. *CrystEngComm* **2011**, *13*, 7202.

(36) Pokroy, B.; Fitch, A.; Zolotoyabko, E. The Microstructure of Biogenic Calcite: A View by High-Resolution Synchrotron Powder Diffraction. *Adv. Mater.* **2006**, *18*, 2363.

**For Table of Contents Only**